A Fast Multipole-Method-Based Calculation of the Capacitance Matrix for Multiple Conductors Above Stratified Dielectric Media

Yuancheng C. Pan, Weng Cho Chew, *Fellow, IEEE*, and L. X. Wan

***Abstract*—An efficient static fast-multipole-method (FMM)-based algorithm is presented in this paper for the evaluation of the parasitic capacitance of three-dimensional microstrip signal lines above stratified dielectric media. The effect of dielectric interfaces on the capacitance matrix is included in the stage of FMM when outgoing multipole expansions are used to form local multipole expansions by the use of interpolated image outgoing-to-local multipole translation functions. The increase in computation time and memory usage, compared to the free-space case, is, therefore, small. The algorithm retains $O(N)$ computational and memory complexity of the free-space FMM, where N is the number of conductor patches.**

I. Introduction

ECENT advances in the very large scale integration (VLSI) technology further the need for fast and accurate calculation of the capacitance and inductance matrices of general three-dimensional (3-D) multiconductor structures in the presence of layered dielectric interfaces. In calculating the capacitance matrix, one attractive approach is to compute the charge densities on the conductor surfaces using an integral equation. The kernel of the integral equation can be the free-space Green's function [1] or the closed-form spatial Green's functions [2]–[5]. This integral-equation method only requires the discretization of the surfaces of the conductors and finite dielectrics and, therefore, is much more efficient than the finite-difference (FD) and finite-element (FE) methods [6]–[8], when the integral equation can be solved at a low computation cost using, for example, the fast multipole method (FMM).

The method of moments (MoM) can be used to solve the integral equation of unknown charge densities by expanding the charge densities with a set of basis functions. The expansion reduces the integral equation to a dense matrix equation that computes a potential vector by multiplying the Green's function matrix with a vector of charges. A rudimentary approach to solving this matrix equation for the vector of charges is by directly inverting the dense Green's function matrix. Such matrix inversion requires $O(N^3)$ operations. The computation cost can be greatly reduced by using an iterative method, which requires $O(N^2)$ operations per iteration. The storage requirement for the matrix is $O(N^2)$.

The evaluation of potentials, done by a matrix–vector multiplication, is often the most expensive part of an iterative method. The static FMM developed by Greengard and Rokhlin performs a matrix–vector product in $O(N)$ calculations [9], [10]. Leathrum and Board produced a parallelized version of this algorithm [11]. Recent work by Nabors and White incorporated static FMM into a fast algorithm for extracting the capacitance matrix of multiple conductors either in a homogeneous dielectric medium [12], [13] or in an arbitrary piecewise-homogeneous dielectric medium [14], [15]. Jandhyala *et al.* extended the static FMM to geometries that have multiple conductors and multiple dielectric interfaces by considering the image charges as additional sources [16], [17].

In this paper, we will also study conductor geometries that include multiple layers of dielectrics with an FMM. The novelty of our method is that the effect of dielectric interfaces are exactly accounted for to within numerical precision. Also, the CPU workload is only slightly more than that of the free-space algorithm. Furthermore, the dielectric interfaces do not affect the stage of recursive division of the space occupied by the conductor structures, the stage of forming outgoing multipole expansions, and the stage of forming local multipole expansions from the parent-level local multipole expansions. The effects of dielectric interfaces to the capacitance matrix are included in the stage when outgoing multipole expansions are used to form local multipole expansions. The bookkeeping of this method, therefore, is quite simple. It also has the advantage that the presence of layered dielectrics and, hence, the presence of image charge panels, does not enlarge the spatial size of the conductor structure needed to be enclosed. This new method retains the $O(N)$ computational complexity of an FMM and has $O(N)$ memory requirement as $N \to \infty$.

II. General Formulation

A system of M arbitrarily shaped 3-D conducting objects is placed above L layers of dielectrics, as depicted in Fig. 1. The layers of dielectrics are infinite in the xy-plane. The analysis of such a structure is important in RF frequency analog circuits and integrated circuits.

Manuscript received October 19, 1999. This work was supported by the Air Force Office of Scientific Research under Multidisciplinary Research Initiative Grant F49620-96-1-0025 and by the Intel Corporation.

The authors are with the Center for Computational Electromagnetics, Department of Electrical and Computer Engineering, University of Illinois, Urbana, IL 61801-2991 USA.

Publisher Item Identifier S 0018-9480(01)01683-0.

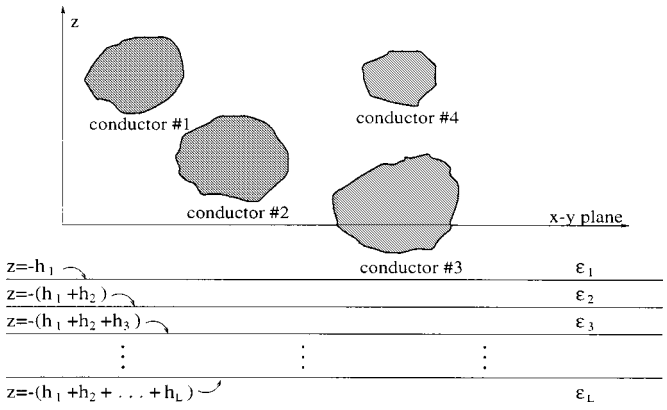

Fig. 1. Multiple conductors lying above stratified dielectric media.

One method of calculating the capacitance matrix is to find the charge distribution $\rho(\mathbf{r})$ on the surfaces of the conductors. The capacitance matrix is defined by the relation

$$Q_n = \sum_{m=1}^{M} C_{nm} V_m \tag{1}$$

where $n = 1, 2, \ldots, M$, Q_n is the total charge on conductor n, and V_m is the voltage on conductor m. The nmth element of the capacitance matrix C_{nm} can be found by calculating Q_n induced on conductor n when conductor m is at 1 V, while all other conductors are at 0 V.

The total charge on conductor n is found by integrating the charge density $\rho_n(\mathbf{r})$ over the surface of the conductor

$$Q_n = \int_{S_n} dS' \, \rho_n(\mathbf{r}') \tag{2}$$

where S_n is the surface of conductor n and the charge density ρ_n is the solution to the integral equation

$$\Psi(\mathbf{r}) = \sum_{n=1}^{M} \int_{S_n} dS' \, \frac{\rho_n(\mathbf{r}')}{|\mathbf{r} - \mathbf{r}'|} + \sum_{i=1}^{\infty} \sum_{n=1}^{M} \int_{S_n^i} dS' \frac{\rho'_{n,i}(\mathbf{r}')}{|\mathbf{r} - \mathbf{r}'|}, \quad \cdot \mathbf{r} \in S_m; \quad m = 1, \ldots, M. \tag{3}$$

In (3), Ψ is the potential, S_n^i is the surface of the ith image of conductor n, and $\rho'_{n,i}$ is the charge density on the ith image of conductor n. The image charge density $\rho'_{n,i}$ is related to the original charge density ρ_n by a scalar factor γ_i given by

$$\rho'_{n,i}(\mathbf{r} + \hat{z}\Delta_{z_i}) = \gamma_i \rho_n(\mathbf{r}). \tag{4}$$

For a dielectric interface at $z = h_1$, with thickness h_2, above ground plane, the scalar factors γ_i are given by

$$\gamma_1 = \frac{\epsilon_0 - \epsilon_2}{\epsilon_0 + \epsilon_2}$$

$$\gamma_i = -\left(\frac{\epsilon_0 - \epsilon_2}{\epsilon_0 + \epsilon_2}\right)^i \frac{2\epsilon_0}{\epsilon_0 + \epsilon_2} \frac{2\epsilon_2}{\epsilon_0 + \epsilon_2}$$

and Δ_{z_i} are given by

$$\Delta_{z_1} = -z - 2h_1$$

$$\Delta_{z_i} = -z - 2h_1 - 2(i-1)h_2$$

where $i = 2, 3, \ldots$.

The surface of the conductors is discretized into N triangular patches using the MoM. For simplicity, we assume $\rho = \rho_l$ is constant on each patch and use the point-matching method. The potential on the lth patch can be written as

$$\Psi_l = \sum_{k=1}^{N} \int_{T_k} dS' \, \frac{\rho_l}{|\mathbf{r}_l - \mathbf{r}'|} + \sum_{i=1}^{\infty} \sum_{k=1}^{N} \int_{T_k^i} dS' \, \frac{\rho'_{l,i}}{|\mathbf{r}_l - \mathbf{r}'|} \tag{5}$$

where T_k is the surface of the kth triangular patch. If (5) is solved for ρ_l when $\Psi_l = 1$ if $T_l \in S_m$, and when $\Psi_l = 0$ if $T_l \notin S_m$, then the nmth element of the capacitance matrix is

$$C_{nm} = \sum_{l,\, T_l \in S_n} \rho_l. \tag{6}$$

Equation (5) can be discretized through the MoM in the form of a matrix equation of unknown ρ_l

$$\boldsymbol{\Psi} = \overline{\mathbf{M}} \cdot \boldsymbol{\rho}. \tag{7}$$

The matrix $\overline{\mathbf{M}}$ in (7) has the elements

$$M_{lk} = \int_{T_k} dS' \, \frac{1}{|\mathbf{r}_l - \mathbf{r}'|} + \sum_{i=1}^{\infty} \int_{T_k^i} dS' \frac{\gamma_i}{|\mathbf{r}_l - \mathbf{r}'|}. \tag{8}$$

When (7) is solved for ρ using the iterative conjugate gradient (CG) method, the computation cost of each iteration is $O(N^2)$. A static FMM can be used to reduce this cost to $O(N)$.

III. Simple View of The Free-Space Static FMM

Consider a group of N charges located within a sphere of radius R_1 around some origin. The potential because of these charges outside of the sphere can be written as an expansion of outgoing spherical harmonics[1] about the origin [18]

$$\Psi(\mathbf{r}) = \sum_{n=0}^{\infty} \sum_{m=-n}^{n} \frac{M_{nm}}{r^{n+1}} Y_{nm}(\theta, \phi) \tag{9}$$

where M_{nm} are the outgoing multipole coefficients given by

$$M_{nm} = \sum_{i=1}^{N} q_i (r'_i)^n Y_{n,-m}(\theta'_i, \phi'_i) \tag{10}$$

and $Y_{nm}(\theta, \phi)$ are the spherical harmonics. The potential can be approximated by summing the expansion to a finite order p

$$\Psi(\mathbf{r}) \approx \sum_{n=0}^{p} \sum_{m=-n}^{n} \frac{M_{nm}}{r^{n+1}} Y_{nm}(\theta, \phi) \tag{11}$$

with an error bound $\propto (R_1/r)^{p+1}$. Suppose we wish to compute the potential at P field points outside of a sphere of radius R_2 about the same origin, with $R_2 > R_1$ (see Fig. 2). The naive direct approach will require NP operations. However, if N and P are very large, and the upper limit for the error bound can be smaller than the specified tolerance for some p such that $(p+1)^2 \ll N, P$, then the potential at P field points can be

[1] $r^{-(n+1)} Y_{nm}(\theta, \phi)$ is known as the outgoing multipole or spherical harmonic expansion because it represents a field that is outgoing and vanishes at infinity.

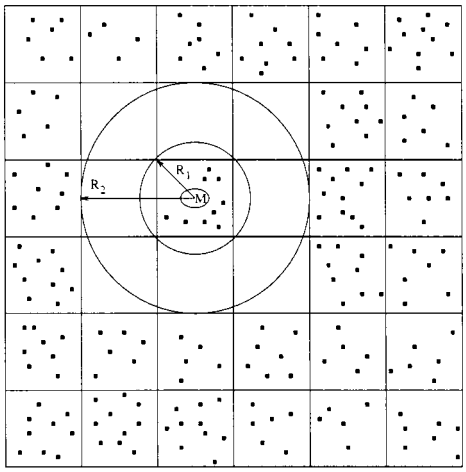

Fig. 2. If the charges are distributed inside the sphere of radius R_1, then the potential at field points outside of the sphere of radius R_2 can be evaluated efficiently by first constructing the outgoing multipole expansion and then applying (11).

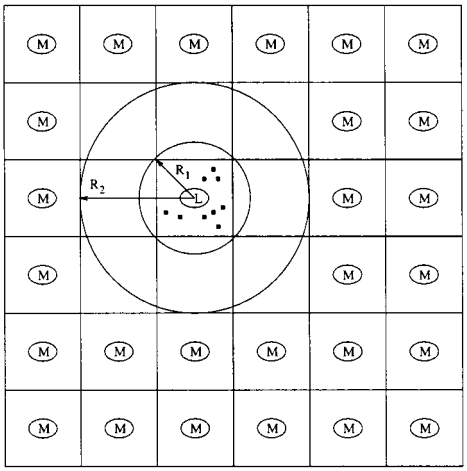

Fig. 3. If the charges are distributed outside of the sphere of radius R_2, then the potential at field points inside of the sphere of radius R_1 can be evaluated efficiently by first separating the charges into small groups, then constructing the outgoing multipole expansion for each group, and then translating the multipole expansions to a local multipole expansion, and then applying (13).

evaluated efficiently by first constructing the order p outgoing multipole expansion in $N(p+1)^2$ operations, and then computing the potential using the outgoing multipole expansion in $P(p+1)^2$ operations. The total operation count of this approach is $(N+P)(p+1)^2 \ll NP$. This is especially true if $R_2 \gg R_1$.

Consider the situation in Fig. 3. There are $\tilde{P}$ boxes, each with an outgoing multipole expansion of order p outside the sphere of radius R_2. We wish to compute the potential due to these outgoing multipole expansions at N field points inside the sphere of radius R_1. It has been shown that, in this case, we can translate the $\tilde{P}$ outgoing multipole coefficients of order p to one local multipole coefficients of the same order using formula

$$L_{jk} = \sum_{i=1}^{\tilde{P}} \sum_{n=0}^{p} \sum_{m=-n}^{n} \alpha_{nm}^{jk}(\mathbf{r}_i) M_{nm}^{(i)}, \qquad j = 0, \ldots, p; \quad k = -j, \ldots, j, \tag{12}$$

and then use the coefficients in the local multipole expansion[2] via the formula

$$\Psi(\mathbf{r}_l') \approx \sum_{j=0}^{p} \sum_{k=-j}^{j} L_{jk} (r_l')^j Y_{jk}(\theta_l', \phi_l'), \qquad l = 1, \ldots, N \tag{13}$$

to evaluate the potential at the N field points within the box inside the circle of radius R_1. The expression for $\alpha_{nm}^{jk}(\mathbf{r}_i)$ in (12) is given in the Appendix. It should be noted that the error bound for using the truncated local multipole expansion is $\propto (R_1/R_2)^{p+1}$. The computation cost is $\tilde{P}(p+1)^4 + N(p+1)^2$ operations. This is much cheaper than a direct calculation.

A simple two-level free-space static FMM is outlined in the following steps to show how outgoing and local multipole expansions can be used to reduce the computation cost of the matrix–vector multiplication in (7).

- Step 1) Box the conductor structure using a cube, and then partition the cube into P equally sized child cubes.
- Step 2) Normalize all distances with respect to the side length of the child cubes.
- Step 3) Take $R_1 = \sqrt{2}/2$ and $R_2 = 1.5$, and determine the order of the outgoing multipole expansion p needed to achieve the desired accuracy.
- Step 4) Calculate outgoing multipole coefficients for each child cube by (10). We call this the aggregation of the different source fields into one common multipole field centered within each box.
- Step 5) Calculate local multipole coefficients by translating the outgoing multipole expansions outside of the sphere of radius R_2 into the circle of radius R_1 (see Fig. 3). This is repeated for each child cube.
- Step 6) For each field point within a child cube, calculate the potential due to charges outside of the sphere of radius R_2 using the local expansion and (13). We call this the disaggregation process, as it is the reverse of the aggregation process.
- Step 7) For each field point in a child cube, calculate directly the potential due to the charges within the given cube and the cubes that are contiguous to the given cube.

The efficiency of the two-level algorithm outlined above can be improved through the use of multilevel algorithms. Detailed description of such algorithms can be found in [10] and [12].

IV. Two-Level Multilayer Static FMM

Because of its simplicity, we will use the two-level algorithm to illustrate the incorporation of layer dielectric effects. When solving a multilayer electrostatic problem using the method of images, the dielectric media are replaced with image charges at appropriate locations. We will not work directly with the image charges. Instead, we will utilize the images of the outgoing multipole expansions to create an efficient FMM algorithm.

Definition 4.1: The ith image cube of a cube is the ith mirror image of the given cube.

The concept of image cube can help us compute the image outgoing multipole expansions from the original outgoing mul-

[2] $(r_l')^j Y_{jk}(\theta_l', \phi_l')$ is known as the incoming or local multipole expansion because it represents an incoming field regular at $r_l' = 0$.

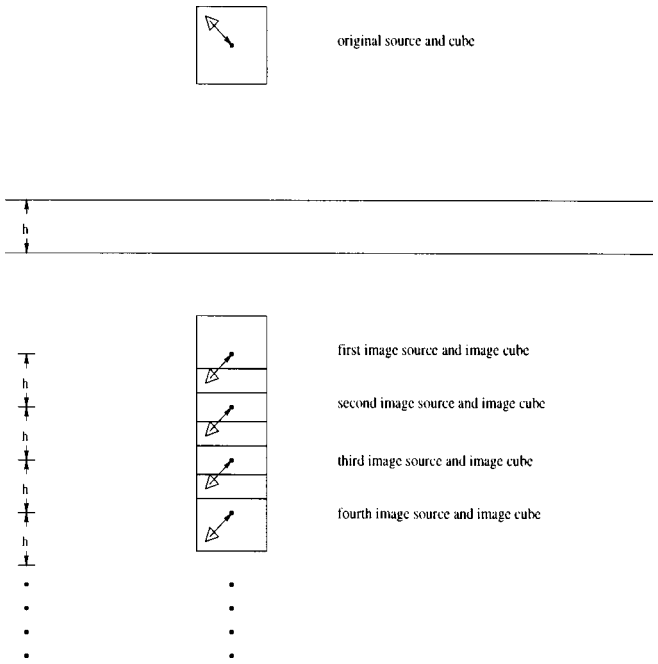

Fig. 4. Image cube is similarly defined as the image charges, i.e., the ith image cube is the ith mirror image of the original cube.

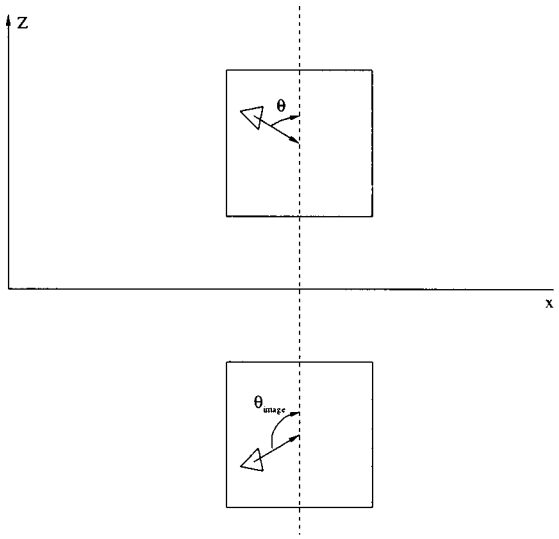

Fig. 5. Multipole expansion of an image charge is formed with zenith angle $\pi - \theta$.

tipole expansion. It is easy to see from Fig. 4 that if an outgoing multipole expansion is constructed from a charge with respect to the center of a cube, then the ith image outgoing multipole expansion of this outgoing multipole expansion is the expansion of the ith image charge with respect to the center of the ith image cube.

In calculating the outgoing multipole expansion of the image charge, we note that the zenith angle between the image charge and image cube center is changed to $\pi - \theta$, as shown in Fig. 5. The normalized (with respect to the side length of the cubes) order nm outgoing multipole expansion of charge q about a cube center is given by

$$M_{nm}(\mathbf{r}) = \frac{q}{a}\left(\frac{r}{a}\right)^n Y_{n,-m}(\theta, \phi) \tag{14}$$

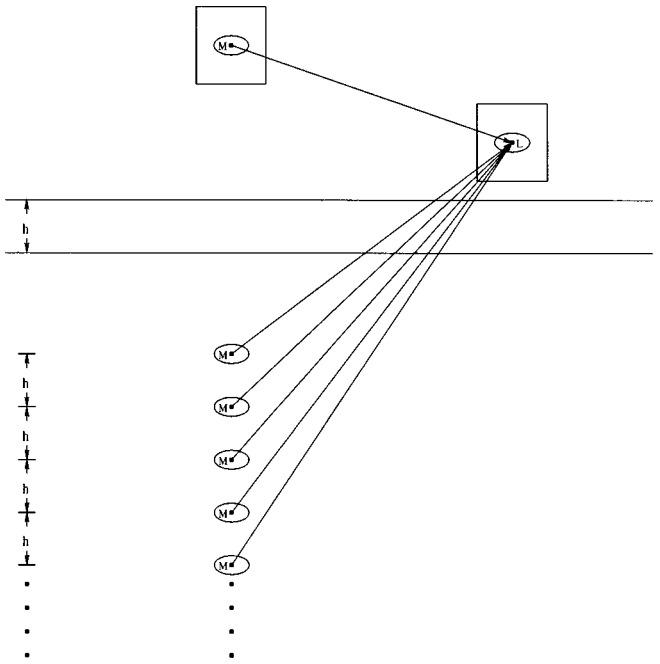

Fig. 6. In the presence of multilayer medium, there are source outgoing-to-local multipole translations as well as image outgoing-to-local multipole translations.

where $\mathbf{r}$ is the vector between q and the cube center and a is the side length of the cubes. The spherical harmonics have the well-known property that

$$Y_{nm}(\theta, \phi) = (-1)^{n+m} Y_{nm}(\pi - \theta, \phi). \tag{15}$$

Using this property, the order nm outgoing multipole expansion of the ith image charge, with strength $\gamma_i q$, about the ith image cube center is

$$\begin{aligned} M_{nm}^i(\mathbf{r}^i) &= \frac{\gamma_i q}{a}\left(\frac{r}{a}\right)^n Y_{n,-m}(\pi - \theta, \phi) \\ &= (-1)^{n+m}\gamma_i M_{nm}(\mathbf{r}). \end{aligned} \tag{16}$$

For a simple two-level multilayer FMM, we can modify Step 5 of the free-space algorithm to include the translations of image outgoing multipole expansions (see Fig. 6). The translation of one outgoing multipole expansion to a local expansion of order jk now takes the form of

$$\begin{aligned} L_{jk} &= \sum_{n=0}^{p}\sum_{m=-n}^{n} \alpha_{nm}^{jk}(r, \theta, \phi) M_{nm} \\ &\quad + \sum_{i=1}^{\infty}\sum_{n=0}^{p}\sum_{m=-n}^{n} \alpha_{nm}^{jk}(r_i, \theta_i, \phi)(-1)^{n+m}\gamma_i M_{nm} \\ &= \sum_{n=0}^{p}\sum_{m=-n}^{n} \alpha_{nm}^{jk}(r, \theta, \phi) M_{nm} \\ &\quad + \sum_{n=0}^{p}\sum_{m=-n}^{n} \tilde{\alpha}_{nm}^{jk}(r_I, \theta_I, \phi) M_{nm}. \end{aligned} \tag{17}$$

Function $\tilde{\alpha}_{nm}^{jk}(r_I, \theta_I, \phi)$ in (17) is defined as

$$\tilde{\alpha}_{nm}^{jk}(r_I, \theta_I, \phi) = \sum_{i=1}^{\infty} \alpha_{nm}^{jk}(r_i, \theta_i, \phi)(-1)^{n+m}\gamma_i. \quad (18)$$

In defining $\tilde{\alpha}_{nm}^{jk}$, we used the fact that $\mathbf{r}_{2,3,\ldots}$ can be determined from $\mathbf{r}_1$ and the dielectric thicknesses. In practice, the infinite sum in (18) can be truncated. Since the absolute value of γ_i monotonically decreases with increasing i, a simple procedure is to neglect images with the absolute value of γ_i less than some preset small value.

V. Multilevel Multilayer Static FMM

The algorithm described in Section IV is quite simple and is for pedagogical purposes. The approach is impractical because computing the outgoing-to-local multipole translation functions α_{nm}^{jk} and $\tilde{\alpha}_{nm}^{jk}$ on the fly is very expensive.

For the discussion of a more sophisticated multilevel algorithm, we need the following definitions from the free-space multilevel FMM.

Definition 5.1: Nearest neighbors of a cube are the same-level cubes that shared at least one corner with a given cube. There are, at most, 26 nearest neighbors to a given cube.

Definition 5.2: Interaction cubes of a cube are the children of the nearest neighbors of the parent of the given cube, excluding the nearest neighbors of the given cube. There are, at most, 189 interaction cubes to a given cube.

In the free-space multilevel FMM, the sources are enclosed in a large cube. This large cube is named the level-0 cube, which is divided into eight equally sized level-1 child cubes. Each child cube is recursively subdivided into smaller cubes until none of the finest level cubes contains more than a fixed number of source patches. The relationships between the cubes are stored in a tree structure.

For a cube on a given level, only the outgoing multipole expansions from the interaction cubes are translated to the local expansion of that cube. In the free-space static FMM, there are 316 possible interaction cube locations (see Fig. 7) and, therefore, 316 unique outgoing-to-local multipole translation matrices. Furthermore, because of the scale-invariance property of electrostatics, one set of this 316 unique outgoing-to-local multipole translation matrices can be used by all levels if outgoing and local multipole expansions are constructed using normalized distances. This set of translation matrices are calculated and stored beforehand. The problem becomes much more complex in the presence of a multilayer dielectric medium. Since the location of the first image of a cube is related to its absolute z-coordinate, for the Lth level of a tree structure, there are approximately $2^L \times 316$ unique image outgoing-to-local multipole translation matrices.

This requirement is evident in Fig. 8, in which two different sections of a tree level are shown with their first images. The outgoing-to-local multipole translations from source cube S to destination cube D and from source cube S' to destination cube D' use the same translation matrix, but because cubes D and D' have different z-coordinates, the outgoing-to-local multipole translations from the image of cube S to cube D and from the image of cube S' to cube D' will use two different matrices.

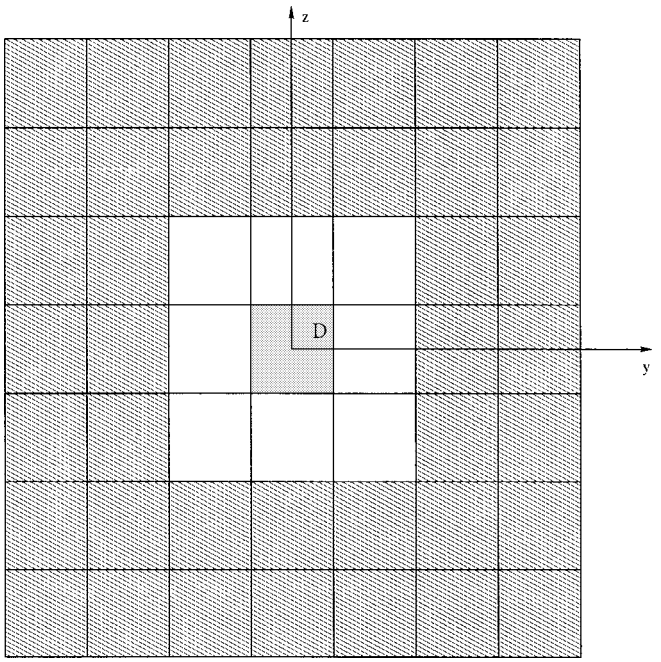

Fig. 7. Shaded cubes are the possible interaction cube locations of cube D when $x = 0$.

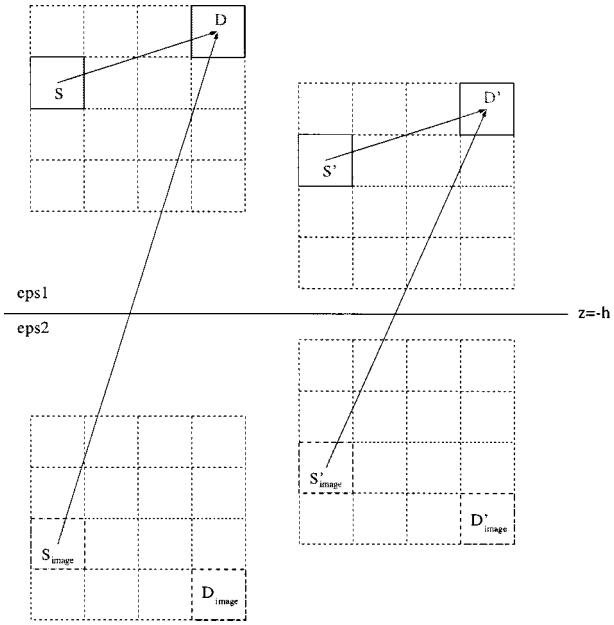

Fig. 8. Relative position of cube S to cube D is the same as cube S' to cube D', but because the absolute coordinates of cube D and cube D' are different, the outgoing-to-local multipole translation from cube S_{image} to cube D is not the same as from cube S'_{image} to cube D'.

There are 2^L possible z-coordinates for level L cube centers, which give rise to $2^L \times 316$ unique matrices for image outgoing-to-local multipole translations. The required number of levels is proportional to $O(\log(N))$; hence, the storage requirement for the image outgoing-to-local multipole translation matrices becomes unacceptable very quickly with the number of unknowns.

To alleviate the excessive memory requirement, the translation function $\tilde{\alpha}_{nm}^{jk}(r_I, \theta_I, \phi)$ is rewritten as $\tilde{\alpha}_{nm}^{jk}(z;\ x, y, l)$.

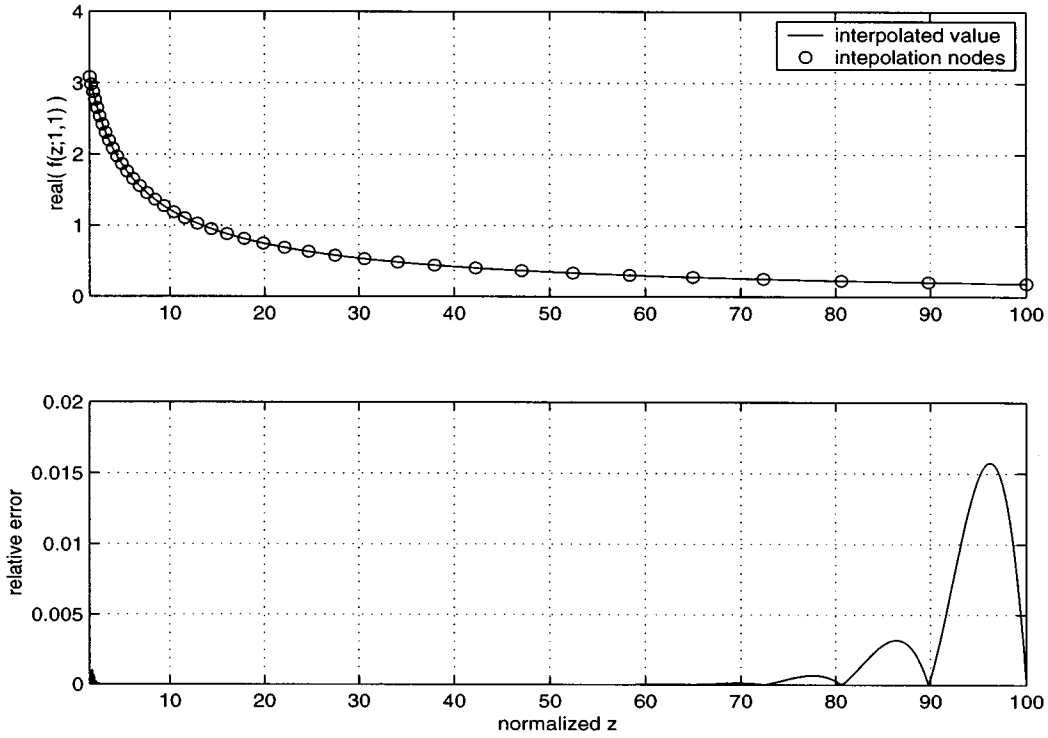

Fig. 9. Accuracy of the interpolation of $f_{00}^{00}(z;\ x = 1.0,\ y = 1.0)$ with 40 nodes.

Here, l is the level number and (x, y, z) is the normalized (with respect to the cube side length of level l) Cartesian representation of (r_I, θ_I, ϕ). There are 49 different $\tilde{\alpha}_{nm}^{jk}(z;\ x, y, l)$ functions for level l, one for each unique combination of (x, y). As mentioned above, computing $\tilde{\alpha}_{nm}^{jk}(z;\ x, y, l)$ on the fly is very computationally intensive. The computational complexity can be greatly reduced with an interpolation technique like the well-known cubic spline function. Since $\alpha_{nm}^{jk}(\mathbf{r})$ is a smooth function that decays rapidly with increases in the magnitude of $\mathbf{r}$, accurate interpolation is possible with logarithmic spacing. A two-interface geometry, with a normalized dielectric thickness of 0.4, is used to illustrate the accuracy of the interpolation. Fig. 9 is a plot of the relative error of interpolating $\tilde{\alpha}_{00}^{00}(z;\ x, y, l)$. A maximum relative error of about 2% was achieved with 40 nodes.

In a free-space static FMM, the memory requirement is $c_1 \cdot N + b$, where $c_1 \sim 4$ kB and $b \sim 8$ MB. In multilayer static FMMs, the memory requirement is $c_1 \cdot N + c_2 \cdot \log(N) + b$. The constant c_2 represents the additional memory requirement for the image terms. The value of c_2 is proportional to the order of multipole expansions and to the number of nodes used to interpolate the image outgoing-to-local multipole translation functions. When the order of multipole expansion is four and the number of interpolation nodes is 40, $c_2 \sim 40$ MB.

VI. Optimizing Multilevel Multilayer Static FMM

The multilevel multilayer static FMM can be optimized in terms of memory use and CPU time.

As mentioned in Section V, when the order of multipole expansion is four and the number of interpolation nodes is 40, $c_2 \sim 40$ MB. This number drops to ~17 MB and ~6 MB for the respective multipole expansion orders of three and two. Since higher order multipole fields decay much faster with distance r than lower order multipole fields, it is memory efficient to interpolate $\tilde{\alpha}_{nm}^{jk}(z;\ x, y, l)$ for $z > 3.0$ and only up to the quadrupole terms. The image outgoing-to-local multipole translation matrices of $\tilde{\alpha}_{nm}^{jk}(r_I, \theta_I, \phi)$ are calculated and stored for the cubes whose normalized center-to-dielectric distance is less than 3.0. It should be pointed out that because these cubes are close to one of the sides of the level-0 cube (see Fig. 10), only partial sets of the 316 image outgoing-to-local multipole translation matrices are required.

To save CPU time, we note that in the free-space algorithm, the maximum normalized distance for an outgoing-to-local multipole translation is $3\sqrt{3}$. In the multilayer algorithm, on the other hand, the distance for an outgoing-to-local multipole translation can be very large, especially for the image of an outgoing multipole expansion that is high above the dielectric interface. When this is the case, we can translate only the monopole and dipole terms of the image outgoing multipole. Since the number of multipoles for an expansion of order p is $(p + 1)^2$, the saving in the number of operations is very significant.

For this algorithm, the worst CPU performance observed is approximately four times that of the free-space algorithm. This is caused mainly by the cubic-spline interpolation. For the most common scenario of a thin microstrip printed on top of a multilayer dielectric medium, the CPU time is less than two times that of the free-space algorithm. If the conductors are far above the dielectric interface, the increase in CPU time is almost negligible.

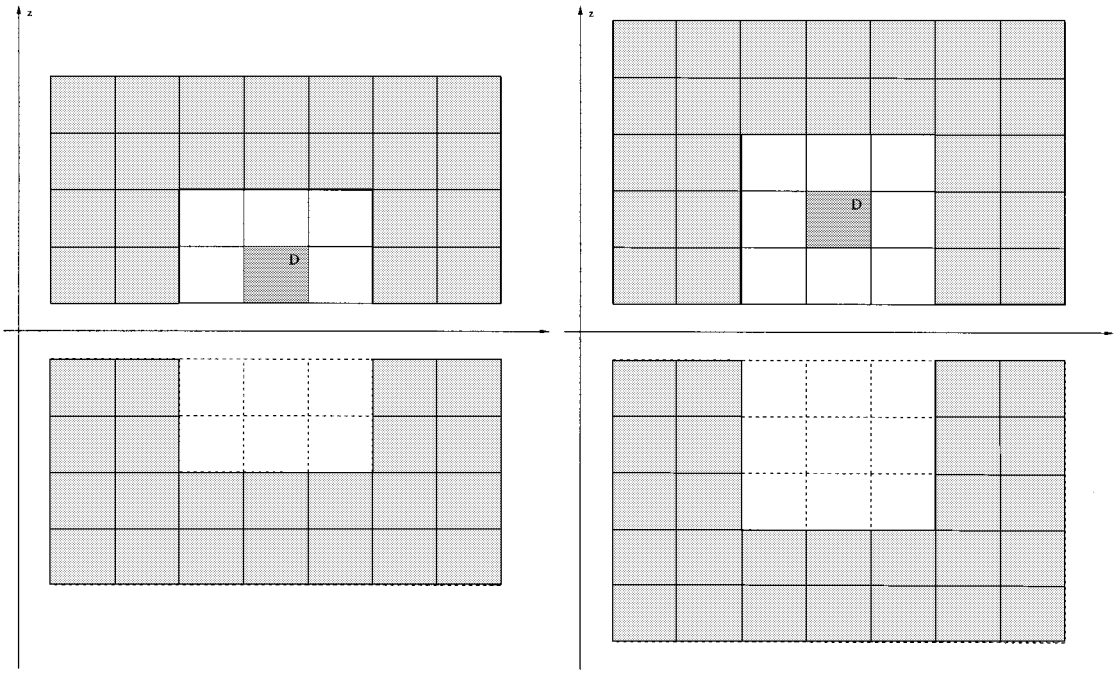

Fig. 10. There are 178 and 218 possible interaction cube locations, respectively, and, therefore, 178 and 218 possible image interaction cube locations for the two layers of cubes that are closest to the dielectric interface.

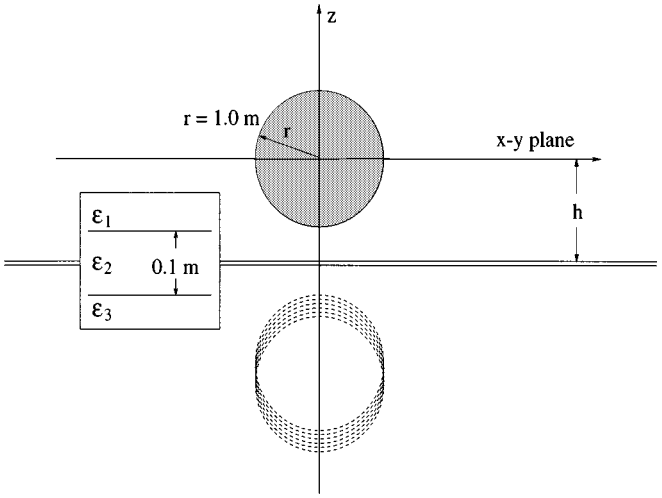

Fig. 11. Conducting sphere lying above two layers of dielectrics.

VII. Numerical Results

The accuracy of the method outlined in the previous section is tested for the case of a unit sphere in the presence of two dielectric interfaces, as shown in Fig. 11. The unit sphere is centered at the origin and is in free space. The first interface occurs at $z = -h$, with $\epsilon_2 = 2.5\epsilon_0$. The second interface occurs at $z = -h - 0.1$. In Fig. 12, the capacitance of the conductor sphere as calculated by the multilevel multilayer static FMM is plotted, along with a plot of the relative error comparing to the values calculated by the MoM. A total of 11 images were included in the calculation, with $\gamma_{11} = -6.3 \times 10^{-3}$. More images can be included at the cost of longer setup time, but the CPU time per iteration will not be affected.

The algorithm is employed to calculate the fringing field effects on the capacitance of a circular microstrip disk with unit radius a (Fig. 13). The accuracy of our method is further verified by comparisons to the numerical results in [19] and the asymptotic formula in [20]. In Tables I–III, rows marked with "NM" are the numerical values taken directly from [19], rows marked with it "AF" are the values computed by the asymptotic formula [20]

$$C \sim \frac{\pi\epsilon_1}{\delta} + 2\epsilon_0 \left[\ln\frac{8}{\delta} - 2 + A\right] + \frac{\delta\epsilon_0}{\pi\epsilon_r}\left[\left(\ln\frac{8}{\delta} + A - 1\right)^2 - 2\right] \tag{19}$$

where A is given by

$$A = -2\epsilon_r \sum_{n=1}^{\infty} \left(\frac{1-\epsilon_r}{1+\epsilon_r}\right)^n \ln(n) + \epsilon_r \ln\pi + (\epsilon_r - 1)\ln 2 + 1 \tag{20}$$

and $\epsilon_r = \epsilon_1/\epsilon_0$, rows marked with "FMM" are the results of the current FMM accelerated numerical method. The values presented in these tables are normalized to the parallel-plate capacitance computed with formula $C = \epsilon_1\pi/\delta$.

Determining the coupling capacitances between signal lines is of special interest to VLSI circuit designers. Fig. 14 depicts a complex geometry consisted of five signal lines. The new FMM-accelerated algorithm was employed to calculated the capacitance matrix when the structure is placed on top of a dielectric slab. The dielectric slab is above the ground plane. The wires have an 1.0 μm $\times$ 0.5 μm cross section. The distances between the wires are 1.0 μm. The dielectric slab has $\epsilon_r = 2.65$. It is of thickness 2.0 μm and supports the conductors. As before, the number of images included is 11. The problem contains 75 318

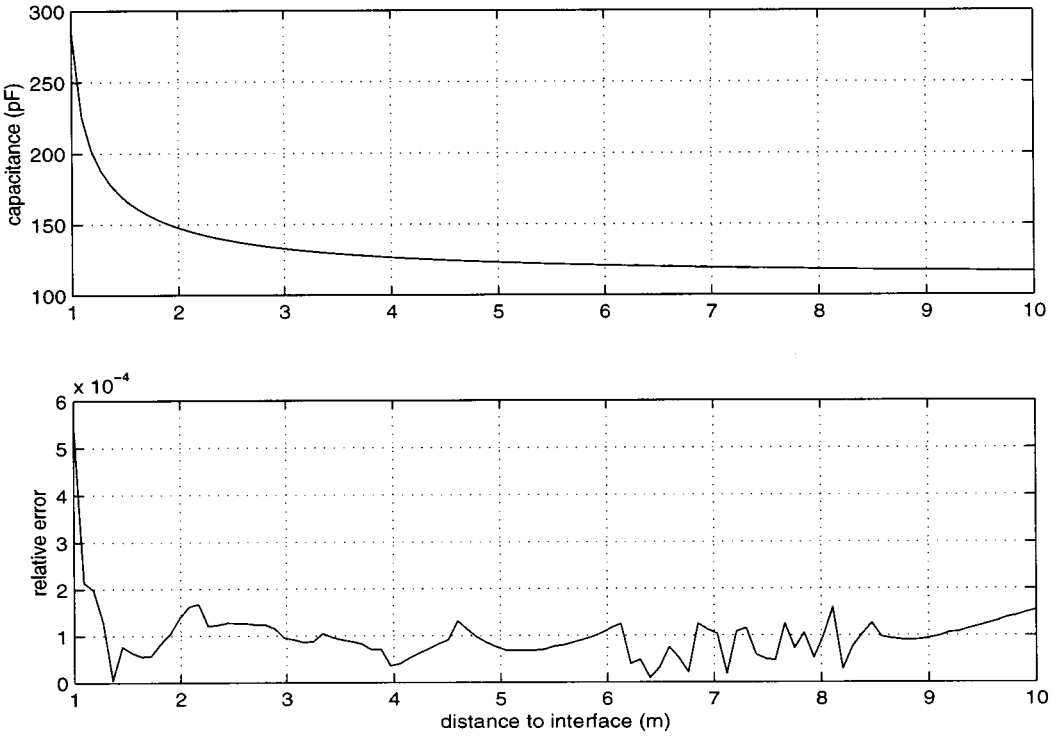

Fig. 12. Capacitance of a sphere with varying distance to the dielectric layers $h_2 = 0.1$ m, $\epsilon_r = 2.65$.

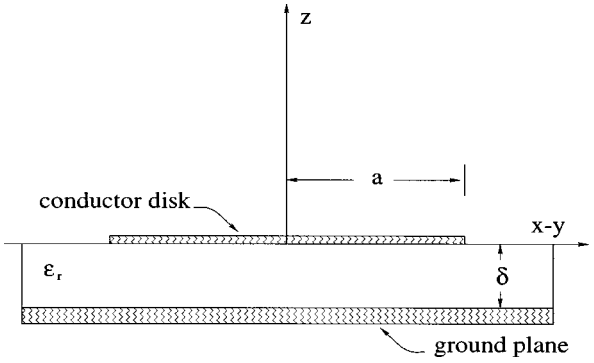

Fig. 13. Circular microstrip disk with radius a is separated from the ground plane by a dielectric substrate with relative permittivity ϵ_r and thickness δ.

TABLE I
NORMALIZED CIRCULAR DISK CAPACITANCE AS A FUNCTION OF d/a FOR $\epsilon_r = 1.0$

δ/a	0.1	0.2	0.3	0.4	0.5	0.6	0.7	0.8	0.9	1.0
AF	1.32	1.57	1.82	2.05	2.27	2.48	2.69	2.89	3.08	3.27
NM	1.32	1.58	1.83	2.08	2.32	2.56	2.80	3.05	3.29	3.53
FMM	1.31	1.57	1.82	2.06	2.31	2.55	2.80	3.04	3.28	3.52

TABLE II
NORMALIZED CIRCULAR DISK CAPACITANCE AS A FUNCTION OF d/a FOR $\epsilon_r = 2.65$

δ/a	0.1	0.2	0.3	0.4	0.5	0.6	0.7	0.8	0.9	1.0
AF	1.18	1.34	1.50	1.65	1.81	1.97	2.13	2.30	2.46	2.63
NM	1.18	1.34	1.50	1.65	1.81	1.97	2.13	2.29	2.45	2.61
FMM	1.17	1.33	1.49	1.64	1.80	1.96	2.12	2.27	2.45	2.61

unknowns, and is solved using six levels. The order for outgoing and local multipole expansions is three. The interpolation of the translation matrices is done by the cubic spline function with 40 nodes. Table IV compares the entries of the capacitance matrix for this structure in free space and in the presence of the dielectric interface. Note that conductor 1 has the air bridge in the middle and conductors 2 and 3 are the straight signal lines.

TABLE III
NORMALIZED CIRCULAR DISK CAPACITANCE AS A FUNCTION OF d/a FOR $\epsilon_r = 9.6$

δ/a	0.1	0.2	0.3	0.4	0.5	0.6	0.7	0.8	0.9	1.0
AF	1.12	1.23	1.34	1.46	1.58	1.71	1.83	1.97	2.10	2.24
NM	1.11	1.23	1.34	1.46	1.58	1.70	1.82	1.94	2.07	2.19
FMM	1.13	1.23	1.34	1.46	1.57	1.69	1.82	1.94	2.06	2.20

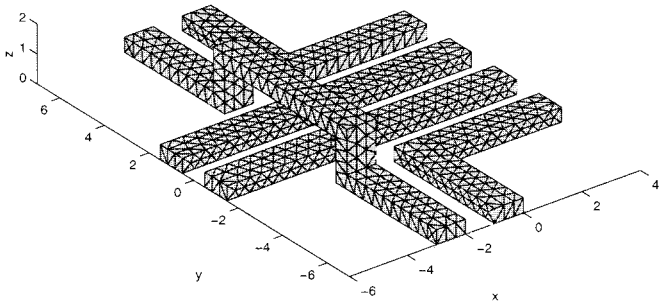

Fig. 14. This conductor geometry is used to demonstrate the ability of the new algorithm to handle complex structures. The signal lines are 1.0 μm in width, and 0.5 μm in height. The distance between the conductors is 1.0 μm.

The efficiency of the method presented in this paper is shown in Figs. 15 and 16, where the CPU time per iteration and the memory usage of the two-layer dielectric medium case is plotted in comparison with the free-space case. This benchmark test was run with a unit-radius conducting sphere above a layer of dielectric material and the ground plane. The center of the sphere is

TABLE IV
EFFECT OF A DIELECTRIC SLAB ABOVE GROUND PLANE ON THE ELEMENTS OF CAPACITANCE MATRIX

	c_{11} (fF)	c_{12} (fF)	c_{13} (fF)	c_{14} (fF)	c_{15} (fF)	CPU time (sec)	memory (MB)
free space	0.4816	-0.0917	-0.0917	-0.0820	-0.0820	6.9	199.5
dielectric	0.7606	-0.0814	-0.0814	-0.0807	-0.0807	53.7	282.1

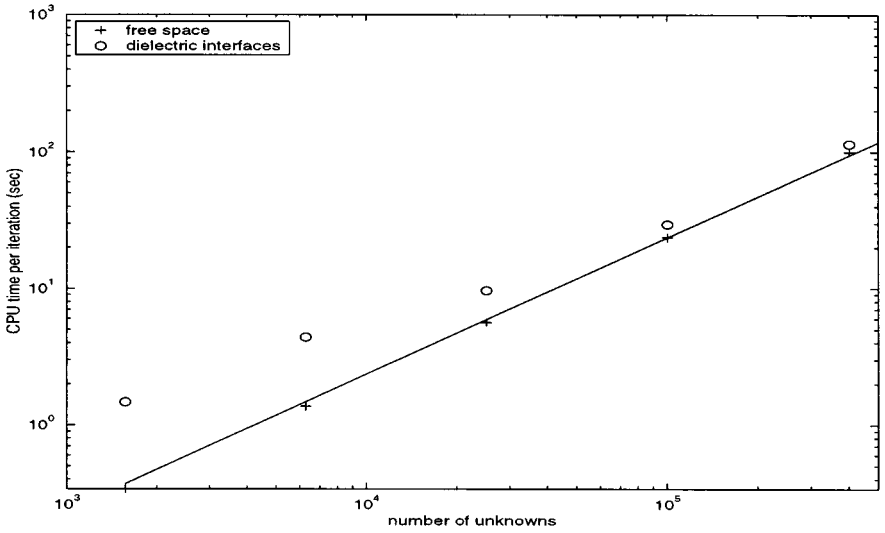

Fig. 15. Computation time of FMM capacitance solvers.

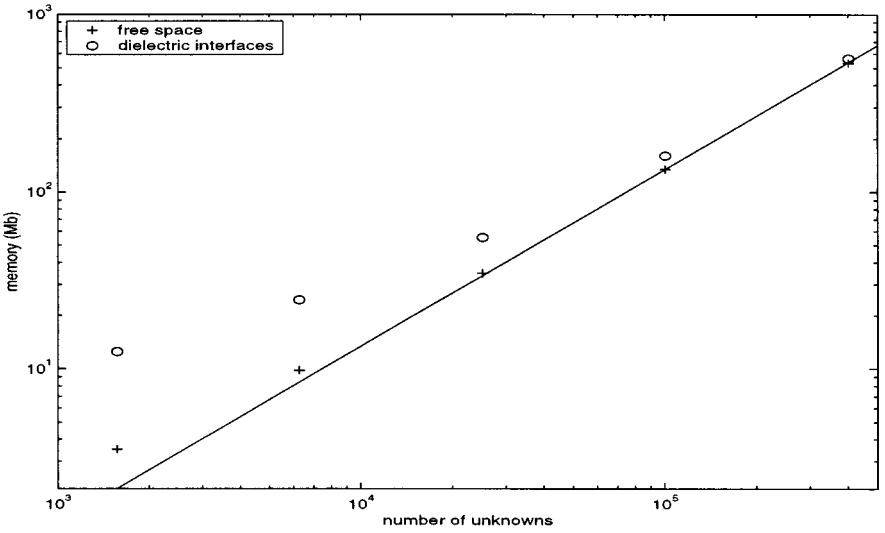

Fig. 16. Memory usage of FMM capacitance solvers.

2.5 m above the dielectric interface. The order for outgoing and local multipole expansions is three. The new method is seen to still have an $O(N)$ computational and memory complexity that approaches $O(N)$ as $N \to \infty$.

The largest case in Figs. 15 and 16 contains 401 408 unknowns. The memory used for the free-space case and the multilayer case were 533 and 565 MB, respectively. This is the limiting case since our DEC Alpha 21164/600 workstations has 512 MB of memory and 1 GB of virtual memory. On a slower SGI Power Challenger that has 2 GB of memory, a sphere consisted of 1 204 352 unknowns were solved using eight levels. The computation took 1391.5 s per iteration and used 1.44 GB of memory. As a comparison, the free-space FMM took 966.8 s per iteration and used 1.39 GB of memory.

This algorithm was coded in C++. Unless otherwise noted, all CPU times in this section were taken from a DEC Alpha 21164/600 workstation.

APPENDIX

Due to the property of the scale invariance of Laplace's equation, it is advantageous to normalize the outgoing and local multipole coefficients on each level with respect to the level's cube size. Let a be the current level cube size and a_c and a_p be the

child and the parent level cube sizes, respectively. With normalized coefficients, we have an order nm outgoing multipole expansion of monopole q

$$M_{nm}(\mathbf{r}) = \frac{q}{a}\left(\frac{r}{a}\right)^n Y_{n,-m}(\theta, \phi). \tag{21}$$

The translation from the order nm child-level outgoing multipole to order jk parent-level outgoing multipole in the first stage of the FMM is governed by

$$\beta_{nm}^{jk}(\mathbf{r}) = \left(\frac{a_c}{a_p}\right)^{j+1} (-1)^{(|k|-|m|-|k-m|)/2} \cdot \sqrt{\binom{j+k}{n+m}\binom{j-k}{n-m}} \left(\frac{r}{a_c}\right)^{j-n} Y_{j-n,\,m-k}(\theta, \phi), \quad \text{if } |m-k| \le j-n. \tag{22}$$

The order nm outgoing multipole to order jk local multipole translation in the second stage of the FMM is governed by

$$\alpha_{nm}^{jk}(\mathbf{r}) = (-1)^{n+(|k-m|-|k|-|m|)/2}\left(\frac{a}{r}\right)^{j+n+1} \cdot \sqrt{\binom{j-k+n+m}{n+m}\binom{j+k+n-m}{n-m}} \cdot Y_{j+n,\,m-k}(\theta, \phi). \tag{23}$$

Finally, the translation from the parent-level order nm local multipole to child-level order jk local multipole in the second stage of the FMM is governed by

$$\beta_{nm}^{jk}(\mathbf{r}) = (-1)^{n+j+(|m|-|m-k|-|k|)/2}\left(\frac{a_c}{a_p}\right)^{n} \cdot \sqrt{\binom{n+m}{j+k}\binom{n-m}{j-k}} \left(\frac{r}{a_c}\right)^{n-j} Y_{n-j,\,m-k}(\theta, \phi), \quad \text{if } |m-k| \le n-j. \tag{24}$$

These formulas were first derived by the Feng [21] and later rederived by Zhao and Chew [22]. They differ from those that exist in the open literature.

REFERENCES

[1] C. Wei, R. F. Harrington, J. R. Mautz, and T. K. Sarkar, "Multiconductor transmission lines in multilayered dielectric media," *IEEE Trans. Microwave Theory Tech.*, vol. MTT-32, pp. 439–450, Apr. 1984.

[2] W. T. Weeks, "Calculation of coefficients of capacitance of multiconductor transmission lines in the presence of a dielectric interface," *IEEE Trans. Microwave Theory Tech.*, vol. MTT-18, pp. 35–43, Jan. 1970.

[3] N. K. Das and D. M. Pozar, "A generalized spectral-domain Green's function for multilayer dielectric substrates with application to multilayer transmission lines," *IEEE Trans. Microwave Theory Tech.*, vol. MTT-35, pp. 326–335, Mar. 1987.

[4] W. Delbare and D. D. Zutter, "Space-domain Green's function approach to the capacitance calculation of multiconductor lines in multilayered dielectrics with improved surface charge modeling," *IEEE Trans. Microwave Theory Tech.*, vol. 37, pp. 1562–1568, Oct. 1989.

[5] K. S. Oh, D. Kuznetsov, and J. E. Schutt-Aine, "Capacitance computations in a multilayered dielectric medium using closed-form spatial Green's functions," *IEEE Trans. Microwave Theory Tech.*, vol. 42, pp. 1443–1453, Aug. 1994.

[6] H. Nelis, E. Deprettere, and P. Dewilde, "An efficient method for modeling VLSI interconnections," in *European Circuit Theory Design Conf.*, Sept. 1989, pp. 94–98.

[7] M. A. Kolbehdari, "VLSI interconnections with a MMTL in a multilayered dielectric media," *J. Electromag. Waves Applicat.*, vol. 10, pp. 1485–1506, 1996.

[8] M. Feliziani and F. Maradei, "Capacitance matrix calculation of a wire conductor line: A new FEM approach," *IEEE Trans. Electromagn. Compat.*, vol. 40, pp. 262–270, Aug. 1998.

[9] L. Greengard and V. Rokhlin, "A fast algorithm for particle simulations," *J. Comput. Phys.*, vol. 73, pp. 325–348, 1987.

[10] L. Greengard, *The Rapid Evaluation of Potential Fields in Particle Systems*. Cambridge, MA: MIT Press, 1988.

[11] J. Leathrum, Jr. and J. Board, "Parallelization of the fast multipole algorithm: Algorithm and architecture design," Ph.D. dissertation, Dept. Comput. Sci., Duke Univ., Durham, NC, 1992.

[12] K. Nabors and J. White, "FastCap: A multipole accelerated 3-D capacitance extraction program," *IEEE Trans. Computer-Aided Design*, vol. 10, pp. 1447–1459, Nov. 1991.

[13] K. Nabors, S. Kim, and J. White, "Fast capacitance extraction of general three-dimensional structures," *IEEE Trans. Microwave Theory Tech.*, vol. 40, pp. 1496–1506, July 1992.

[14] K. Nabors and J. White, "Multipole-accelerated capacitance extraction algorithms for 3-D structures with multiple dielectrics," *IEEE Trans. Circuits Syst. I*, vol. 39, pp. 946–954, Nov. 1992.

[15] J. Tausch and J. White, "Capacitance extraction of 3-D conductor systems in dielectric media with high-permittivity ratios," *IEEE Trans. Microwave Theory Tech.*, vol. 47, pp. 18–26, Jan. 1999.

[16] V. Jandhyala, E. Michielssen, and R. Mittra, "Multipole-accelerated capacitance computation for 3-D structures in a stratified dielectric medium using a closed-form Green's function," *Int. J. Microwave Millimeter-Wave Computer-Aided Eng.*, vol. 5, pp. 68–78, May 1995.

[17] ——, "Memory-efficient, adaptive algorithm for multipole-accelerated capacitance computation in a stratified dielectric medium," *Int. J. Microwave Millimeter-Wave Computer-Aided Eng.*, vol. 6, pp. 381–390, Nov. 1996.

[18] J. D. Jackson, *Classical Electrodynamics*, 2nd ed. New York: Wiley, 1975.

[19] W. C. Chew and J. A. Kong, "Effects of fringing fields on the capacitance of circular microstrip disk," *IEEE Trans. Microwave Theory Tech.*, vol. MTT-28, pp. 98–104, Feb. 1980.

[20] ——, "Microstrip capacitance for a circular disk through matched asymptotic expansions," *SIAM J. Appl. Math.*, vol. 42, Apr. 1982.

[21] S. C. Feng, "private communication," unpublished, 1982.

[22] J. S. Zhao and W. C. Chew, "Three dimensional multilevel fast multipole algorithm from static to electrodynamic," *Microwave Opt. Technol. Lett.*, vol. 26, no. 1, pp. 43–48, July 2000.

Yuancheng C. Pan received the B.Sc. degree in electrical engineering with additional majors in mathematics and physics and the M.Sc. degree from the University of Wisconsin-Madison, in 1994 and 1995, respectively, and is currently working toward the Ph.D. degree at University of Illinois at Urbana-Champaign.

From 1996 to 1998, he was an Electrical Engineer with Agilent Technologies (formerly the Microwave Instrument Division, Hewlett–Packard Company). Since 1998, he has been a Research Assistant in the Department of Electrical Engineering, University of Illinois at Urbana-Champaign. His current research interests are in numerical methods for circuit parameter extraction.

Mr. Pan is a member of Phi Kappa Phi.

Weng Cho Chew (S'79–M'80–SM'86–F'93) received the B.S., M.S., and Engineer's degrees from the Massachusetts Institute of Technology, Cambridge, in 1976, 1978, and 1980, respectively, all in electrical engineering.

From 1981 to 1985, he was with Schlumberger-Doll Research, Ridgefield, CT. While with Schlumberger-Doll Research, he was also a Professor at the University of Illinois at Urbana-Champaign, where he continues to teach graduate courses in waves and fields in inhomogeneous media and the theory of microwave and optical waveguides, and supervises a graduate research program. From 1989 to 1993, he was the Associate Director of the Advanced Construction Technology Center, University of Illinois at Urbana-Champaign, and is currently the Director of the Center for Computational Electromagnetics and the Electromagnetics Laboratory at the same University. He has authored *Waves and Fields in Inhomogeneous Media* (New York: Van Nostrand, 1990), authored or co-authored over 200 scientific journal papers, and presented over 270 conference papers. His recent research interest has been in the area of wave propagation, scattering, inverse scattering, and fast algorithms related to scattering, inhomogeneous media for geophysical sub surface sensing, and nondestructive testing applications. He has previously analyzed electrochemical effects and dielectric properties of composite materials, microwave and optical waveguides, and microstrip antennas. He is an Associate Editor for the *Journal of Electromagnetic Waves and Applications* (1996–present) and *Microwave Optical Technology Letters* (1996–present). He was an Associate Editor for the *International Journal of Imaging Systems and Technology* (1989–1994), and has been a Guest Editor for the *Journal of Imaging Systems and Technology* (1989), and *Electromagnetics* (1995). His name is listed in the University of Illinois at Urbana-Champaign's *List to Excellent Instructors*.

Dr. Chew is a member of Eta Kappa Nu, Tau Beta Pi, URSI Commissions B and F, and the Society of Exploration Geophysics. He was an AdCom member of the IEEE Geoscience and Remote Sensing Society, and is currently an associate editor of the IEEE TRANSACTIONS OF GEOSCIENCE AND REMOTE SENSING (1984–present). He was a 1986 National Science Foundation (NSF) Presidential Young Investigator and was the recipient of the 2000 IEEE Graduate Teaching Award. He is a Founder Professor of the College of Engineering, University of Illinois at Urbana-Champaign.

L. X. Wan, photograph and biography not available at time of publication.